29 Azzi S, Blaise A, Steunou V *et al*: Complex tissue-specific epigenotypes in Russell–Silver Syndrome associated with 11p15 ICR1 hypomethylation. *Hum Mutat* 2014; **35**: 1211–1220.
30 Berend SA, Horwitz J, McCaskill C, Shaffer LG: Identification of uniparental disomy following prenatal detection of Robertsonian translocations and isochromosomes. *Am J Hum Genet* 2000; **66**: 1787–1793.
31 Ioannides Y, Lokulo-Sodipe K, Mackay DJ, Davies JH, Temple IK: Temple syndrome: improving the recognition of an underdiagnosed chromosome 14 imprinting disorder: an analysis of 51 published cases. *J Med Genet* 2014; **51**: 495–501.
32 Hosoki K, Kagami M, Tanaka T *et al*: Maternal uniparental disomy 14 syndrome demonstrates Prader–Willi syndrome-like phenotype. *J Pediatr* 2009; **155**: 900–903.
33 Wang JC, Passage MB, Yen PH, Shapiro LJ, Mohandas TK: Uniparental heterodisomy for chromosome 14 in a phenotypically abnormal familial balanced 13/14 Robertsonian translocation carrier. *Am J Hum Genet* 1991; **48**: 1069–1074.
34 Kagami M, Yamazawa K, Matsubara K *et al*: Placentomegaly in paternal uniparental disomy for human chromosome 14. *Placenta* 2008; **29**: 760–761.

Supplementary Information accompanies this paper on European Journal of Human Genetics website (http://www.nature.com/ejhg)

Journal of Human Genetics (2014), 1–5

www.nature.com/jhg

SHORT COMMUNICATION

Silver–Russell syndrome without body asymmetry in three patients with duplications of maternally derived chromosome 11p15 involving *CDKN1C*

Shinichi Nakashima[1], Fumiko Kato[1], Tomoki Kosho[2], Keisuke Nagasaki[3], Toru Kikuchi[4], Masayo Kagami[5], Maki Fukami[5] and Tsutomu Ogata[1]

We report duplications of maternally derived chromosome 11p15 involving *CDKN1C* encoding a negative regulator for cell proliferation in three Japanese patients (cases 1 and 2 from family A and case 3 from family B) with Silver–Russell syndrome (SRS) phenotype lacking hemihypotrophy. Chromosome analysis showed 46,XX,der(16)t(11;16)(p15.3;q24.3)mat in case 1, 46, XY,der(16)t(11;16)(p15.3;q24.3)mat in case 2 and a *de novo* 46,XX,der(17)t(11;17)(p15.4;q25.3) in case 3. Genomewide oligonucleotide-based array comparative genomic hybridization, microsatellite analysis, pyrosequencing-based methylation analysis and direct sequence analysis revealed the presence of maternally derived extra copies of the distal chromosome 11p involving the wild-type *CDKN1C* (a ~7.98 Mb region in cases 1 and 2 and a ~4.43 Mb region in case 3). The results, in conjunction with the previous findings in patients with similar duplications encompassing *CDKN1C* and in those with intragenic mutations of *CDKN1C*, imply that duplications of *CDKN1C*, as well as relatively mild gain-of-function mutations of *CDKN1C* lead to SRS subtype that usually lack hemihypotrophy.
Journal of Human Genetics (2014) **00**, 1–5. doi:10.1038/jhg.2014.100

INTRODUCTION

Silver–Russell syndrome (SRS) is a congenital developmental disorder characterized by pre- and postnatal growth failure, relative macrocephaly, hemihypotrophy and fifth-finger clinodactyly.[1] Recent studies have shown that epimutation (hypomethylation) of the paternally derived *H19*-differentially methylated region (DMR) at the imprinting control region 1 (ICR1) on chromosome 11p15.5 and maternal uniparental disomy 7 account for ~45 and ~5% of SRS patients, respectively.[1] Thus, underlying (epi)genetic factors still remain to be clarified in a substantial fraction of SRS patients, although several rare (epi)genetic aberrations have been identified in a small fraction of SRS patients.[1]

CDKN1C (cyclin-dependent kinase inhibitor 1C) is a maternally expressed gene that resides at the ICR2 just proximal to the ICR1.[2] *CDKN1C* encodes a negative regulator for cell proliferation and, consistent with this, loss-of-function mutations of *CDKN1C* cause Beckwith–Wiedemann syndrome associated with overgrowth.[2,3] Furthermore, recent studies have shown that gain-of-function mutations of *CDKN1C* result in IMAGe syndrome (IMAGeS) characterized by intrauterine growth restriction, metaphyseal dysplasia, adrenal hypoplasia congenita and male genital abnormalities,[2] whereas less severe gain-of-function mutations of *CDKN1C* have been identified in a large family with maternally inherited SRS.[4] Thus, it has been suggested that relatively severe and mild *CDKN1C* gain-of-function effects lead to IMAGeS and SRS, respectively.[4,5] Notably, IMAGeS patients satisfy the diagnostic criteria for SRS proposed by Nechine *et al.*[5,6] and IMAGeS and SRS patients with *CDKN1C* mutations invariably lack hemihypotrophy characteristic of SRS.[4–6]

Here, we report three patients with SRS and duplications of maternally derived chromosome 11p15.5 involving *CDKN1C*. The results, in conjunction with previous findings, imply that duplications of *CDKN1C*, as well as relatively mild gain-of-function mutations of *CDKN1C* lead to SRS subtype that usually lack hemihypotrophy.

CASE REPORTS

Patients

We studied three Japanese patients (cases 1–3) from two families (Figure 1). Cases 1–3 satisfied the SRS diagnostic criteria proposed by Netchine *et al.*,[6] although they lacked hemihypotrophy (Table 1, see its footnote for Netchine SRS criteria). Oligohydramnios characteristic of SRS[7] was also noticed during the pregnancies of cases 2 and 3. They exhibited no IMAGeS-like phenotypes such as radiologically discernible skeletal dysplasia, an episode suggestive of adrenal dysfunction or undermasculinized genitalia in male case 2.

[1]Department of Pediatrics, Hamamatsu University School of Medicine, Hamamatsu, Japan; [2]Department of Human Genetics, Shinshu University School of Medicine, Matsumoto, Japan; [3]Department of Pediatrics, Niigata University School of Medicine, Niigata, Japan; [4]Department of Pediatrics, Saitama Medical University, Saitama, Japan and [5]Department of Molecular Endocrinology, National Research Institute for Child Health and Development, Tokyo, Japan
Correspondence: Professor T Ogata, Department of Pediatrics, Hamamatsu University School of Medicine, 1-20-1, Handayama, Higashi-ku, Hamamatsu, Shizuoka 431-3192, Japan.
E-mail: tomogata@hama-med.ac.jp
Received 10 October 2014; revised 28 October 2014; accepted 31 October 2014

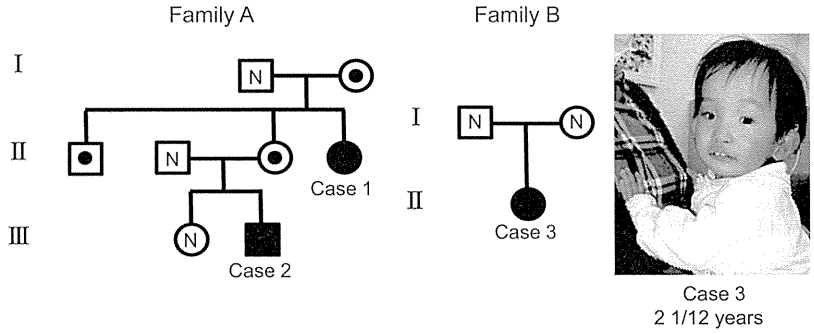

Figure 1 The pedigrees of families A and B and a photograph of case 3. In family A, cases 1 and 2 have an unbalanced translocation involving the distal part of chromosome 11p, the mothers of cases 1 and 2, as well as the brother of case 1 have a balanced translocation involving the distal part of chromosome 11p and the remaining subjects have a normal karyotype. In family B, case 3 has an unbalanced translocation involving the distal part of chromosome 11p and the parents have a normal karyotype. Case 3 exhibits SRS-compatible phenotypes such as prominent forehead, triangular face with relative macrocephaly and micrognathia, ear anomalies and short and curved fifth fingers, but is free from hemihypotrophy.

Table 1 Clinical features of cases 1–3 and reported cases with duplications of maternally derived chromosome 11p15 involving *CDKN1C*

	Case 1 family A female	*Case 2 family A male*	*Case 3 family B female*	*Reported cases (n = 16)*[11–19]
SRS phenotype				
Mandatory criteria for SRS				
BL and/or BW ⩽ −2 SDS	+	+	+	16/16
Scoring system criteria for SRS				
Relative macrocephaly at birth[a]	Unknown	+	+	11/11
PH ⩽ −2 SDS at ⩾ 2 years	+	Unknown	+	14/14
Prominent forehead	+	+	+	8/9
Body asymmetry	−	−	−	1/15
Feeding difficulties	+	−	Unknown	6/6
Other findings				
Gestational age (weeks)	39	32	32	22–38
Oligohydramnios	Unknown	+	+	Unknown
BL, cm (SDS)	38.0 (−4.9)	34.0 (−3.3)	32.0 (−3.9)	N.D.[b]
BW, kg (SDS)	1.3 (−5.3)	0.87 (−3.6)	0.82 (−3.7)	N.D.[b]
BOFC, cm (SDS)	29.5 (−2.7)	28.3 (−0.6)	27 (−1.2)	N.D.[b]
Present age (years:months)	14:00	1:03	3:03	1–31
PH, cm (SDS)	130.7 (−4.7)	60.8 (−6.4)	70.7 (−6.7)	N.D.[b]
PW, kg (SDS)	37.5 (−1.2)	4.8 (−5.3)	6.8 (−4.0)	N.D.[b]
BMI, kg m^{-2} (SDS)	22.0 (0.7)	13.1 (−2.8)	13.6 (−1.5)	N.D.[b]
POFC, cm (SDS)	Unknown	45.0 (−0.5)	48.5 (−0.1)	N.D.[b]
Relative macrocephaly at present[c]	Unknown	+	+	14/15
Triangular face	−	+	+	12/16
Ear anomalies	−	−	+	8/11
Irregular teeth	Unknown	+	+	1/2
Clinodactyly	+	+	+	10/11
Brachydactyly	+	+	−	4/5
Simian crease	+	+	−	1/2
Muscular hypotonia	Unknown	+	+	4/7
Developmental/speech delay	+	+	+	11/15
IMAGe syndrome phenotype				
IUGR	+	+	+	16/16
Metaphyseal dysplasia	−	−	−	Not described
Adrenal hypoplasia	−	−[d]	−[e]	Not described
Genital abnormality	Female	−	Female	Not described

The diagnosis of Silver–Russell syndrome is made when a patient is positive for the mandatory criteria and at least three of the five scoring system criteria (Netchine *et al*.[5])
Abbreviations: BL, birth length; BMI, body mass index; BOFC, birth occipitofrontal circumference; BW, birth weight; IMAGe, intrauterine growth restriction, metaphyseal dysplasia, adrenal hypoplasia congenita and male genital abnormalities; IUGR, intrauterine growth retardation; N.D., not determined; PH, present height; POFC, present occipitofrontal circumference; PW, present weight; SDS, standard deviation score.
For reported cases, the denominators indicate the number of patients examined for the presence or absence of each feature, and the numerators represent the number of patients assessed to be positive for that feature.
Birth and present body sizes were assessed by the gestational/postnatal age- and sex-matched Japanese reference data from the Ministry of Health, Labor and Welfare and from the Ministry of Education, Science, Sports and Culture.
[a]BL or BW (SDS)—BOFC (SDS) ⩽ −1.5.
[b]N.D. because of various ethnicities of affected individuals and descriptions of height assessment (percentile and SDS).
[c]PH or PW (SDS)—POFC (SDS) ⩽ −1.5.
[d]A rapid adrenocorticotropin stimulation test (0.25 mg m^{-2} bolus i.v.; blood sampling at 0 and 60 min) showed a sufficient cortisol response (14.2 → 26.2 μg dl^{-1}) (reference range > 20 μg dl^{-1}).
[e]A growth hormone releasing peptide 2 stimulation test (2 μg kg^{-1} bolus i.v.; blood sampling at 0, 15, 30, 45 and 60 min) yielded a sufficient cortisol response (18.4 → 25.5 μg dl^{-1}).

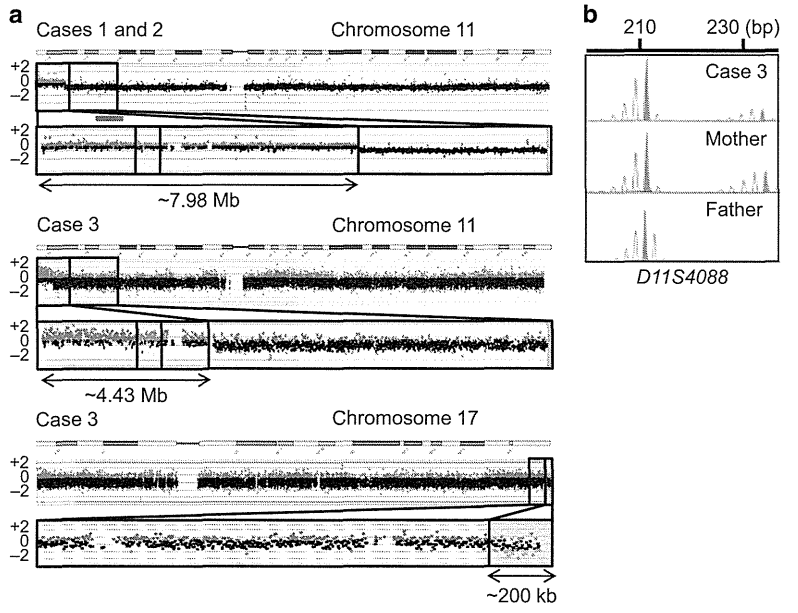

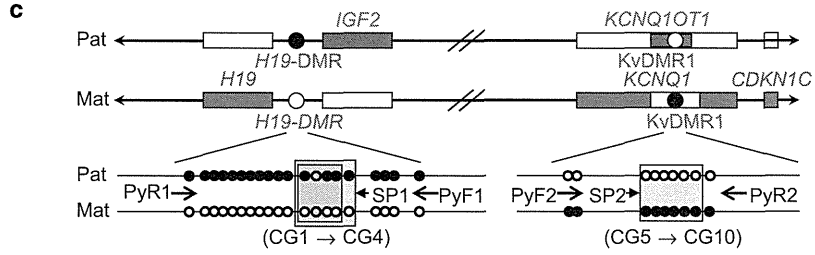

	Case 1			Case 2			Case 3			Controls (n=50)
	P	F	M	P	F	M	P	F	M	Median (Range)
CG1	30	41	53	34	52	55	29	44	44	45 (36 ~ 55)
CG2	31	42	54	37	54	55	28	43	44	46 (36 ~ 57)
CG3	33	45	56	38	57	60	31	47	46	50 (39 ~ 64)
CG4	33	44	55	39	56	57	31	48	46	48 (37 ~ 60)
CG5	72	56	56	72	56	57	68	56	57	58 (49 ~ 66)
CG6	78	59	59	73	59	60	71	61	58	61 (52 ~ 68)
CG7	67	52	50	66	50	52	61	50	49	48 (41 ~ 54)
CG8	69	55	53	68	53	55	63	52	52	48 (42 ~ 55)
CG9	78	60	61	75	63	61	72	63	59	67 (55 ~ 72)
CG10	74	63	57	79	60	59	77	63	64	64 (55 ~ 71)

Figure 2 Representative molecular findings. (**a**) Array comparative genomic hybridization analysis. The black, red and green dots represent signals indicative of the normal, increased (log2 signal ratio > +0.5) and decreased (log2 signal ratio < −0.8) copy numbers, respectively. The log2 signal ratios of +0.5 and −1.0 indicate the presence of three copies and a single copy of the corresponding regions, respectively. The red and the green rectangles represent increased and decreased copy number regions, respectively. The yellow rectangles denote the regions encompassing the ICR1 and the ICR2. (**b**) Microsatellite analysis for *D11S4088* proximal to the KvDMR1. Unequal amplification of the heterozygous peaks in each subject is consistent with short products being more easily amplified than long products and comparison of area under curves of the 212 bp and the 234 bp alleles between case 3 and the mother indicates the presence of two 212 bp alleles and a single 234 bp allele in case 3. This implies that the maternal 212 and 234 bp alleles and the paternal 212 bp allele have been transmitted to case 3. (**c**) Pyrosequencing-based methylation analysis of the *H19*-DMR at the ICR1 and the KvDMR1 at the ICR2, using bisulfite-treated genomic DNA. The cytosine residues at the CpG dinucleotides within the *H19*-DMR is methylated after paternal transmission (filled circles) and unmethylated after maternal transmission (open circles), whereas those within the KvDMR1 is unmethylated after paternal transmission (open circles) and methylated after maternal transmission (filled circles). Paternally and maternally expressed genes are shown in blue and red, respectively. For the *H19*-DMR, a segment encompassing 21 CpG dinucleotides was PCR amplified with PyF1 and PyR1 primers and a sequence primer (SP1) was hybridized to a single-stranded PCR product. Subsequently, the MIs were obtained for four CpG dinucleotides (CG1–CG4) (indicated with a yellow rectangle). The blue rectangle indicates the CTCF binding site 6. The CpG dinucleotide between CG1 and CG2 was not examined, because it constitutes a C/T SNP (indicated with gray circles). The KvDMR1 was similarly examined using PyF2 and PyR2 primers and SP2 and the MIs were obtained for CG5–CG10. The MIs are summarized in the bottom table. F, father; and M, mother; P, patient.

Cytogenetic and molecular studies

This study was approved by the Institute Review Board Committee at Hamamatsu University School of Medicine and was performed using peripheral leukocyte samples and primers shown in Supplementary Table S1 after obtaining written informed consent. The methods for molecular studies were as reported previously.[7] We also obtained written informed consent to publish the facial photograph of case 3 from the parents.

Chromosome analysis showed 46,XX,der(16)t(11;16)(p15.3;q24.3) mat in case 1, 46,XY,der(16)t(11;16)(p15.3;q24.3)mat in case 2 and a *de novo* 46,XX, der(17)t(11;17)(p15.4;q25.3) in case 3 (Figure 1). Then, genomewide oligonucleotide-based array comparative genomic hybridization was carried out using a catalog human array (2×400 K format, ID G4448A) (Agilent Technologies), revealing the presence of three copies of the distal parts of chromosome 11p involving the ICR1 and the ICR2 in cases 1–3 (a ~7.98 Mb region in cases 1 and 2 and a ~4.43 Mb region in case 3) (Figure 2a). No discernible deletion was identified on the distal chromosome 16q in cases 1 and 2, indicating the position of the chromosome 16q breakpoint at the very telomeric portion, whereas a ~200 kb deletion was detected in the telomeric portion of chromosome 17q in case 3. There was no other copy number alteration that was not registered in the Database of Genomic Variants (http://dgv.tcag.ca/dgv/app/home). Microsatellite analysis was carried out for four loci on the duplicated chromosome 11p, showing the presence of two alleles of maternal origin and a single allele of paternal origin in cases 1–3 (Figure 2b and Supplementary Table S2). Subsequently, pyrosequencing-based methylation analysis was performed for four CpG dinucleotides (CG1–CG4) within the *H19*-DMR and six CpG dinucleotides (CG5–CG10) within the KvDMR1 using bisulfite-treated leukocyte genomic DNA samples and methylation index (MI, the ratio of methylated clones) was obtained for each of CG1–CG10 using PyroMark Q24 (Qiagen) (Figure 2c). In cases 1–3, the MIs for CG1–CG4 were mildly decreased or around the lower limit of the normal range and those for CG5–CG10 were mildly increased or around the upper limit of the normal range. Direct sequence analysis showed no discernible mutation on the *CDKN1C* coding region.

DISCUSSION

Cases 1–3 had SRS without hemihypotrophy (body asymmetry) in the presence of maternally derived extra copies of the distal chromosome 11p involving the ICR1 and the ICR2. This implies that the SRS phenotype lacking hemihypotrophy in cases 1–3 is primarily caused by two copies of maternally expressed genes on the two ICRs. In this regard, of duplicated maternally expressed genes, *CDKN1C* functions as a negative growth regulator[8] and *CDKN1C* gain-of-function mutations have been identified in SRS and IMAGeS,[2,4,5] whereas neither *H19* nor *KCNQ1* appears to have a positive role in growth regulation. Indeed, *H19* is regarded as a possible tumor suppressor gene[9] and *KCNQ1* encoding a voltage-gated potassium channel is involved in cardiac arrhythmias.[10] Thus, it is likely that SRS phenotype lacking hemihypotrophy in cases 1–3 is primarily caused by the presence of two functional copies of the wild-type *CDKN1C*. It should be pointed out, however, that although the der(16)t(11;16)(p15.3;q24.3) chromosome in cases 1 and 2 had no discernible chromosome 16q deletion, the der(17)t(11;17)(p15.4;q25.3) chromosome in case 3 was missing the ~200 kb telomeric 17q region that harbors several genes. In addition, there are multiple nonimprinted genes on the duplicated chromosome 11p15 regions. Thus, altered dosage of such genes may have exerted a certain effect on growth patterns of cases 1–3.

An extra copy of maternally derived chromosome 11p15 involving *CDKN1C* has been identified in 16 patients (Table 1) (for detailed clinical features of each case, see Supplementary Table S3).[11–19] Notably, although they frequently show SRS-like phenotype, hemihypotrophy (body asymmetry) has been found only in a single case[12] and none of them exhibit IMAGeS-like skeletal, adrenal or genital manifestation. This provides further support for the notion that two copies of maternally derived *CDKN1C*, as well as mild gain-of-function mutations of *CDKN1C* usually lead to SRS subtype lacking hemihypotrophy.

CONFLICT OF INTEREST

The authors declare no conflict of interest.

ACKNOWLEDGEMENTS

This work was supported by Grants-in-Aid for Scientific Research (A) (25253023) and Research (B) (23390083) from the Japan Society for the Promotion of Science, by Grants for Research on Intractable Diseases (H22-161) from the Ministry of Health, Labor and Welfare (MHLW) and by Grant for National Center for Child Health and Development (25-10).

1 Eggermann, T. Russell-Silver syndrome. *Am. J. Med. Genet. C Semin. Med. Genet.* **154C**, 355–364 (2010).
2 Arboleda, V.A., Lee, H., Parnaik, R., Fleming, A., Banerjee, A. & Ferraz-de-Souza, B. *et al.* Mutations in the PCNA-binding domain of CDKN1C cause IMAGe syndrome. *Nat. Genet.* **44**, 788–792 (2012).
3 Soejima, H. & Higashimoto, K. Epigenetic and genetic alterations of the imprinting disorder Beckwith–Wiedemann syndrome and related disorders. *J. Hum. Genet.* **58**, 402–409 (2013).
4 Brioude, F., Oliver-Petit, I., Blaise, A., Praz, F., Rossignol, S. & Le Jule, M. *et al.* CDKN1C mutation affecting the PCNA-binding domain as a cause of familial Russell Silver syndrome. *J. Med. Genet.* **50**, 823–830 (2013).
5 Kato, F., Hamajima, T., Hasegawa, T., Amano, N., Horikawa, R. & Nishimura, G. *et al.* IMAGe syndrome: clinical and genetic implications based on investigations in three Japanese patients. *Clin. Endocrinol.* **80**, 706–713 (2014).
6 Netchine, I., Rossignol, S., Dufourg, M. N., Azzi, S., Rousseau, A. & Perin, L. *et al.* 11p15 imprinting center region 1 loss of methylation is a common and specific cause of typical Russell-Silver syndrome: clinical scoring system and epigenetic-phenotypic correlations. *J. Clin. Endocrinol. Metab.* **92**, 3148–3154 (2007).
7 Fuke, T., Mizuno, S., Nagai, T., Hasegawa, T., Horikawa, R. & Miyoshi, Y. *et al.* Molecular and clinical studies in 138 Japanese patients with Silver–Russell syndrome. *PLoS ONE* **8**, e60105 (2013).
8 Lee, M. H., Reynisdottir, I. & Massague, J. Cloning of p57(KIP2), a cyclin-dependent kinase inhibitor with unique domain structure and tissue distribution. *Genes Dev.* **9**, 639–649 (1995).
9 Hao, Y., Crenshaw, T., Moulton, T., Newcomb, E. & Tycko, B. Tumour-suppressor activity of H19 RNA. *Nature* **365**, 764–767 (1993).
10 Wang, Q., Curran, M. E., Splawski, I., Burn, T. C., Millholland, J. M. & VanRaay, T. J. *et al.* Positional cloning of a novel potassium channel gene: KVLQT1 mutations cause cardiac arrhythmias. *Nat. Genet.* **12**, 17–23 (1996).
11 Fisher, A. M., Thomas, N. S., Cockwell, A., Stecko, O., Kerr, B. & Temple, I. K. *et al.* Duplications of chromosome 11p15 of maternal origin result in a phenotype that includes growth retardation. *Hum. Genet.* **111**, 290–296 (2002).
12 Eggermann, T., Meyer, E., Obermann, C., Heil, I., Schüler, H. & Ranke, M. B. *et al.* Is maternal duplication of 11p15 associated with Silver–Russell syndrome? *J. Med. Genet.* **42**, e26 (2005).
13 Schönherr, N., Meyer, E., Roos, A., Schmidt, A., Wollmann, H. A. & Eggermann, T. *et al.* The centromeric 11p15 imprinting centre is also involved in Silver–Russell syndrome. *J. Med. Genet.* **44**, 59–63 (2007).
14 South, S. T., Whitby, H., Maxwell, T., Aston, E., Brothman, A. R. & Carey, J. C. Co-occurrence of 4p16.3 deletions with both paternal and maternal duplications of 11p15: modification of the Wolf–Hirschhorn syndrome phenotype by genetic alterations predicted to result in either a Beckwith–Wiedemann or Russell–Silver phenotype. *Am. J. Med. Genet. A* **146A**, 2691–2697 (2008).
15 Bliek, J., Snijder, S., Maas, S. M., Polstra, A., van der Lip, K. & Alders, M. *et al.* Phenotypic discordance upon paternal or maternal transmission of duplications of the 11p15 imprinted regions. *Eur. J. Med. Genet.* **52**, 404–408 (2009).

16 Eggermann, T., Spengler, S., Bachmann, N., Baudis, M., Mau-Holzmann, U. A. & Singer, S. *et al.* Chromosome 11p15 duplication in Silver-Russell syndrome due to a maternally inherited translocation t(11;15). *Am. J. Med. Genet. A* **152A**, 1484–1487 (2010).
17 Cardarelli, L., Sparago, A., De Crescenzo, A., Nalesso, E., Zavan, B. & Cubellis, M. V. *et al.* Silver-Russell syndrome and Beckwith–Wiedemann syndrome phenotypes associated with 11p duplication in a single family. *Pediatr. Dev. Pathol.* **13**, 326–330 (2010).
18 Bonaldi, A., Mazzeu, J. F., Costa, S. S., Honjo, R. S., Bertola, D. R. & Albano, L. M. *et al.* Microduplication of the ICR2 domain at chromosome 11p15 and familial Silver-Russell syndrome. *Am. J. Med. Genet. A* **155A**, 2479–2483 (2011).
19 Chiesa, N., De Crescenzo, A., Mishra, K., Perone, L., Carella, M. & Palumbo, O. *et al.* The KCNQ1OT1 imprinting control region and non-coding RNA: new properties derived from the study of Beckwith-Wiedemann syndrome and Silver–Russell syndrome cases. *Hum. Mol. Genet.* **21**, 10–25 (2012).

Supplementary Information accompanies the paper on Journal of Human Genetics website (http://www.nature.com/jhg)

ELSEVIER

Brain & Development xxx (2014) xxx–xxx

BRAIN & DEVELOPMENT
Official Journal of the Japanese Society of Child Neurology

www.elsevier.com/locate/braindev

Original article

Episodic tremors representing cortical myoclonus are characteristic in Angelman syndrome due to *UBE3A* mutations

Masahide Goto [a,*], Yoshiaki Saito [a], Ryoko Honda [a], Takashi Saito [a], Kenji Sugai [a], Yuko Matsuda [a], Chiharu Miyatake [a], Eri Takeshita [a], Akihiko Ishiyama [a], Hirofumi Komaki [a], Eiji Nakagawa [a], Masayuki Sasaki [a], Chieko Uto [b], Kenjiro Kikuchi [c], Takahiro Motoki [d], Shinji Saitoh [e]

[a] *Department of Child Neurology, National Center of Neurology and Psychiatry, Tokyo, Japan*
[b] *Department of Pediatrics, Isawa-Kyoritu Hospital, Yamanashi, Japan*
[c] *Division of Neurology, Saitama Children's Medical Center, Saitama, Japan*
[d] *Department of Pediatrics, Uwajima City Hospital, Ehime, Japan*
[e] *Department of Pediatrics and Neonatology, Nagoya City University Graduate School of Medical Sciences, Nagoya, Japan*

Received 14 February 2014; received in revised form 7 April 2014; accepted 9 April 2014

Abstract

Objective: Neurological manifestations including psychomotor developmental delay and epilepsy in patients with Angelman syndrome caused by ubiquitin protein ligase E3A (*UBE3A*) mutations has been considered similar but is relatively milder than that in patients with deletion-type Angelman syndrome. This makes the diagnosis of the former subgroup often difficult. We here characterized epilepsy, specifically the types of tremulous movement, in 4 patients (age, 3–38 years) with Angelman syndrome caused by *UBE3A* mutations.

Methods: Ictal electroencephalography was used to record episodic tremors in all study patients. Jerk-locked averaging was performed using digital electroencephalography and surface electromyogram data from patients who were monitored for 24 h.

Results: All patients had tremors in the limbs, head, and trunk, which resulted in 2 patients falling backward. These tremors lasted several seconds, and could emerge in clusters for hours in older patients. In addition, the tremors coincided with 7–8 Hz rhythmic activity with a frontocentral predominance, diffuse spike-wave bursts, or no apparent change on electroencephalography. In 2 patients, these tremors were confirmed as cortical myoclonus using jerk-locked averaging. The other seizure types were isolated generalized myoclonus and tonic seizures. None of the patients experienced atypical absence seizures. Levetiracetam therapy was effective in controlling the myoclonic events in 2 of the 3 patients.

Conclusion: Semirhythmic myoclonus is common in patients with Angelman syndrome caused by *UBE3A* mutations, and such myoclonic events are often life disabling. The preserved expression of gamma-aminobutyric acid type A receptor subunit genes located proximal to *UBE3A* might explain the low prevalence of absence seizures in this population.

Keywords: Jerk-locked averaging; Levetiracetam; Myoclonic absence; Tremor; *UBE3A* mutations

1. Introduction

Angelman syndrome (AS) is characterized by severe psychomotor retardation, epilepsy, ataxia, involuntary

* Corresponding author. Address: Department of Child Neurology, National Center of Neurology and Psychiatry, 4-1-1 Ogawahigashi-cho, Kodaira, Tokyo 187-8551, Japan. Tel.: +81 42 341 2711; fax: +81 42 346 1705.
E-mail address: masapon.go@gmail.com (M. Goto).

http://dx.doi.org/10.1016/j.braindev.2014.04.005
0387-7604/

Please cite this article in press as: Goto M et al. Episodic tremors representing cortical myoclonus are characteristic in Angelman syndrome due to *UBE3A* mutations. Brain Dev (2014), http://dx.doi.org/10.1016/j.braindev.2014.04.005

or jerking movements, and a happy disposition accompanied with inappropriate bursts of laughter. This syndrome can result from the following genetic mechanisms: (1) deletions within a critical region of 15q11.2–q13 on the maternal chromosome (70% of AS cases), (2) paternal uniparental disomy (2–3%), (3) imprinting defects in maternal DNA methylation (3–5%), and (4) mutations within the ubiquitin protein ligase E3A gene (*UBE3A*), which localizes to the 15q11.2–q13 region on the maternal chromosome (5–10%) [1]. Genes that encode gamma-aminobutyric acid type A receptor ($GABA_AR$) subunits are also located in 15q11.2–q13, and defects in these subunits may account for the increased prevalence of severe epileptic seizures in patients with deletion-positive AS compared with those with mutation-positive AS [2]. Seizure patterns are usually similar across all individuals with AS, and myoclonic and atypical absence seizures are common in those with *UBE3A* deletions and mutations [3]. Because few studies have reported ictal electroencephalographic findings in individuals with *UBE3A* mutations, we aimed to characterize the epileptic events in this population.

Limb tremors are characteristic of AS. Using jerk-locked averaging (JLA), these tremors can be identified as cortical myoclonus when they occur simultaneously with rhythmic activity (5–10 Hz) in the frontocentral brain regions [4]. However, tremors that occur during postural tasks have not been associated with changes on electroencephalography (EEG) and back-averaging analysis [5]. In addition, patients with AS often experience myoclonic jerks [6,7], with ictal EEG revealing diffuse 1–3 Hz slow waves in the presence or absence of spike components. Myoclonus is typically synchronous with the spiking activity [6] or rarely occurs in conjunction with paroxysms but without synchronicity with the spikes [5,7]. In the present study, we aimed to characterize epileptic events in patients with AS caused by *UBE3A* mutations and to classify the characteristic tremors of AS according to ictal EEG and JLA results of these patients.

2. Methods

2.1. Subjects

Four of the 24 patients with AS (18 cases with deletions in the 15q11.2–q13 chromosomal region, as indicated by fluorescence in situ hybridization, 1 case with a methylation defect, and 5 cases with a *UBE3A* mutation) who visited our hospital between 2002 and 2012 were enrolled in this study. The characteristics of these 4 patients are shown in Table 1. All clinical materials used in this study were obtained for diagnostic purposes with informed consent.

2.2. Electrophysiological studies

Three patients were monitored using a 24-h EEG video, whereas ictal EEG was performed for the remaining 1 patient during a prolonged tremulous event. Digital electroencephalographic recording was not available for this patient. The Neurofax video-EEG system (Nihon Kohden, Tokyo, Japan) was used to record activities on ictal EEG and electromyography (EMG) that were sampled digitally at 1000 Hz and band-pass filtered (0.53–300 Hz). Recording electrodes were placed on the scalp according to the international 10–20 system, and electromyographic activity was recorded simultaneously from the deltoid or forearm muscles bilaterally and was rectified for analysis. In 1 patient, head tremors predominated during recording, and surface electromyographic activity recorded from the limb muscles failed to show a level of activity sufficient for back-averaging analysis. Thus, JLA was performed in 2 patients using SSE-V500 computer software (Gram Corporation, Saitama, Japan). To analyze cortical potentials before EMG, $\geqslant 50$ artifact-free segments of EEG and EMG were collected and averaged for each ictal event.

2.3. Genetic studies

Genomic DNA was extracted from patient blood samples. All *UBE3A*-coding exons and flanking sequences were amplified by PCR and sequenced directly using an ABI PRISM 310 system and the primers described by Lossie et al. [2]. All base positions were based on GenBank® accession No. U84404.1.

3. Results

All 4 patients were born to unrelated, healthy parents following an uncomplicated pregnancy and delivery. There was no family history of intellectual disability or epilepsy. Delayed psychomotor development was suspected during late infancy when each patient gained the ability to crawl and to sit unsupported at the age of 10–11 months. Independent walking was achieved in 3 patients between 1 year and 6 months and 4 years of age; however, these patients never gained the ability to utter meaningful words. Furthermore, computed tomography and/or magnetic resonance imaging revealed nonspecific findings. Genetic analysis of *UBE3A* identified heterozygous mutations in each patient, including a common 6-base in-frame deletion in patients 2 and 4 (Table 1).

The patients exhibited tremors in the limbs, head, and/or trunk, which usually persisted up to 10 s and occurred in clusters spanning several hours. Consciousness was preserved during these episodes (Supplementary Videos 1 and 2). The tremulous events

Please cite this article in press as: Goto M et al. Episodic tremors representing cortical myoclonus are characteristic in Angelman syndrome due to *UBE3A* mutations. Brain Dev (2014), http://dx.doi.org/10.1016/j.braindev.2014.04.005

Table 1
Characteristics of patients with Angelman syndrome caused by *UBE3A* mutations.

Patient	1	2	3	4
Age/Sex/Body Weight	3 years/M/15 kg	15 years/F/69 kg	3 years/M/12 kg	38 years/F/64 kg
Happy disposition	+	+	+	+
Meaningful words	None	None	None	None
Microcephaly	–	–	+	+
Ataxic gait	+	+	+	+
Social smile	2 months	3 months	3 months	3 months
Head control	3 months	3 months	3 months	3 months
Sitting unsupported	6 months	9 months	11 months	1 year
Crawling	10 months	10 months	1 year 6 months	NA
Independent walking	1 year 6 months	4 years	-	3 years 8 months
Developmental quotient#	79 (3 years)	12 (15 years)	29 (3 years)	NA
UBE3A mutation	Exon 16 c3134G>A; p.G850S	Exon 16 c.3090_3095delCTTAAA; p.853_854delLK	Exon 15 c.3020_3021delGA; p.E812fs	Exon 16 c.3090_3095delCTTAAA; p.853_854delLK

NA: data not available.
#: Assessed by the Kinder Infant Developmental Scale (KIDS score, issued by the Center of Developmental Education and Research, Tokyo, Japan, 1989).

occasionally resulted in backward falls in patients 1 and 3. During the tremulous events in each patient, surface EMG revealed semirhythmic (6–10 Hz) contractions occurring simultaneously over 50- to 200-ms periods between agonist and antagonist arm muscles. Ictal EEG showed 7–8 Hz rhythmic activity with a frontocentral predominance (Figs. 1A and B, 2A and 3) in all patients, in addition to diffuse spike-wave bursts (Fig. 1A) in patients 1 and 4. On some occasions, no apparent change was evident on EEG (Fig. 2B) in patient 2.

Surface electromyographic activity did not correlate with frontocentral rhythmic activity or the spike components of diffuse spike-wave bursts. In patient 1, JLA revealed positive peaks over centroparietal areas that preceded bursts of electromyographic activity that coincided with frontocentral 7–8 Hz rhythmic activity and diffuse spike-wave bursts by approximately 15 and 105 ms, respectively (Fig. 1C). In patient 2, JLA without electroencephalographic alterations generated a reproducible positive–negative biphasic potential over the contralateral hemisphere, with a centroparietal predominance. Similar results were obtained during myoclonic tremors demonstrating 8–10 Hz rhythmic activity. A positive peak (i.e., at the onset of the negative slope) preceded tremors by 13 ms. The tremors were not controlled completely with antiepileptics, but levetiracetam administration in 2 of the 3 patients and ethosuximide in 1 patient ameliorated the myoclonic events (Table 2).

4. Discussion

The patients presented here did not exhibit any of the interictal EEG findings typical of AS, including 2–3 Hz high amplitude rhythmic activity over the frontal regions, prolonged runs of rhythmic 4–6 Hz theta activity with centrotemporal emphasis, or 3–5 Hz rhythmic activity with occipital predominance [8]. However, a happy disposition, intellectual disabilities with severe speech impairment, and, in particular, the presence of tremors prompted us to analyze the *UBE3A* sequence, which confirmed AS diagnosis. In this study, we identified cortical potentials that preceded tremors in patients with AS carrying *UBE3A* mutations. Our findings demonstrated that the tremors were cortical myoclonus, and our findings were consistent with those of previous reports on similar movement disorders caused by genetic deletions in patients with AS. In another study, cortical myoclonus was present in 13 of 14 patients with AS carrying *UBE3A* mutations [9], which might be an important disease indicator for proper AS diagnosis in this population. In addition, we reported for the first time that semirhythmic myoclonus without apparent electroencephalographic changes or with concomitant diffuse spike-wave bursts exhibits JLA findings that are common to myoclonus with frontocentral rhythmic activity. Thus, tremors occurring with AS may be classified as (1) postural tremors without electroencephalographic changes or prior cortical potentials [5,10], (2) cortical myoclonus without electroencephalographic changes, (3) cortical myoclonus with frontocentral 8–10 Hz rhythmic activity, or (4) cortical myoclonus with diffuse spike-wave discharge. In addition, the last item in this classification might correspond to myoclonic absence seizures in AS. However, this may not apply to the ictal symptoms of patient 1. Because the diffuse spike-wave phase was relatively short in this patient, consciousness was difficult to assess during intense generalized myoclonus, thereby resulting in backward falls in the patient.

Please cite this article in press as: Goto M et al. Episodic tremors representing cortical myoclonus are characteristic in Angelman syndrome due to *UBE3A* mutations. Brain Dev (2014), http://dx.doi.org/10.1016/j.braindev.2014.04.005

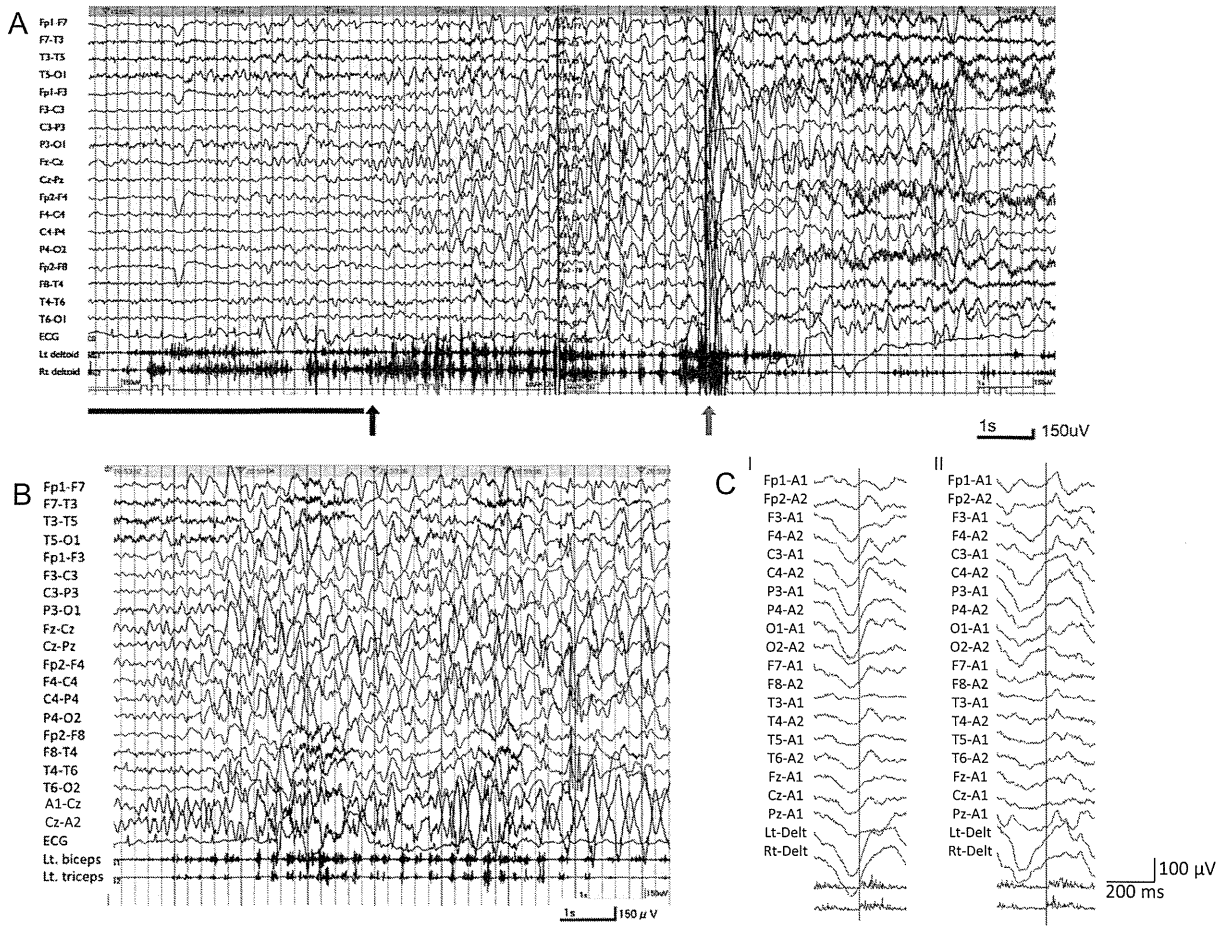

Fig. 1. Ictal electroencephalography (EEG) of patient 1. Tremors appeared (bar) when the patient was walking while holding onto a wall. Motion arrest (black arrow) was followed by intensified trembling, a backward fall (gray arrow), and crying. The initial ictal phase involved 8–10 Hz rhythmic activity with a frontocentral predominance, which evolved into 2.5–4 Hz slow activity with spike components (A). Surface EMG revealed 6–10 Hz semirhythmic simultaneous contractions (50–100 ms) between his biceps and triceps during tremors (B). Back averaging of cortical activity time locked to the onset of tremors in the right deltoid muscle in patient 1 (C). I: Averaging during 8–10 Hz rhythmic activity with an Fz predominance. II: Averaging during 2.5–4 Hz diffuse activity. For each analysis, $\geqslant$50 artifact-free segments were collected from several ictal events. In both instances (I and II), the distribution of positive peaks over centroparietal areas preceded electromyographic activity by approximately 15 and 105 ms, respectively.

Epilepsy with myoclonic absence (EMA) is an epileptic syndrome characterized by rhythmic myoclonus and 3 Hz diffuse spike-wave bursts lasting 10–60 s [11]. In patient 1, progressive elevation of the upper extremities during the ictal event was characteristic of EMA. However, myoclonic jerks in EMA are strictly time locked to the spike components observed on EEG, which was not the case in this patient. Interestingly, the latency between the preceding positive potential peak and the electromyographic activity was longer during the spike-wave phase than during the initial phase of central rhythmic activity in this patient. Although the exact cause of this difference in latency remains unclear, the pathomechanisms controlling the myoclonic absence seizures in patients with AS [12] and patients with EMA might be different.

The prolonged myoclonic episodes observed in patients 2 and 4 were similar to the "myoclonic status in nonprogressive encephalopathies (MSNEs)" that complicates AS and other syndromes. However, ictal electroencephalograms recorded in patients with deletion-type AS during MSNEs have been described as generalized spike-wave activity [6,12], which may be regarded as myoclonic absence seizures. Myoclonic events associated with little generalized spike-wave activity may be characteristic of patients with AS carrying *UBE3A* mutations. In fact, atypical absence seizures were reported in 8 of 16 [13], 4 of 4 [14], and 10 of 11 [15] patients with status epilepticus (SE) and deletion-type AS. In contrast, absence SE has been reported in only 1 patient with AS carrying *UBE3A* mutations, which could be defined as dialeptic SE because 8–9.5 Hz

Please cite this article in press as: Goto M et al. Episodic tremors representing cortical myoclonus are characteristic in Angelman syndrome due to *UBE3A* mutations. Brain Dev (2014), http://dx.doi.org/10.1016/j.braindev.2014.04.005

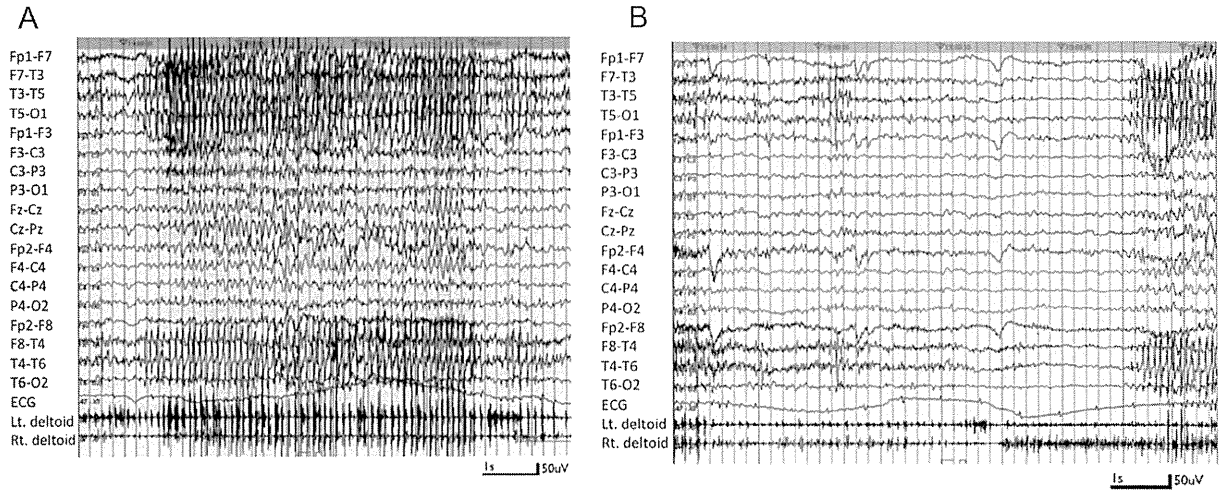

Fig. 2. EEG of patient 2. EEG revealed 8–10 Hz rhythmic activity with an Fz–Cz predominance (A) or no apparent change (B) during the ictal event. Motion artifacts were observed at the temporal areas in A and B.

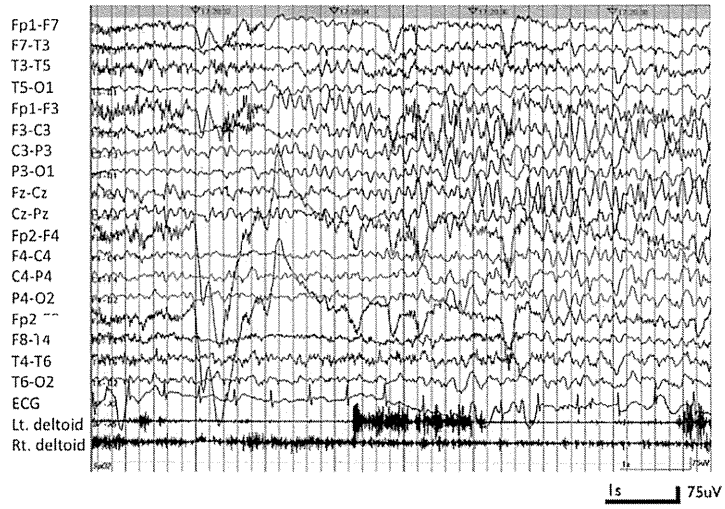

Fig. 3. EEG of patient 3. Head tremors coincided with 6–7 Hz rhythmic activity with a left frontal predominance. Electrodes did not reveal limb tremors in this recording. Jerk-locked averaging was not performed in this patient.

frontal rhythmic activity was present on ictal EEG [16]. Conversely, myoclonic SE in 3 of 3 [17], severe episodes of myoclonus in 4 of 4 [9], and MSNE in 3 [7] patients with AS carrying *UBE3A* mutations were the main types of SE. Although absence seizures are common in patients with AS carrying *UBE3A* mutations, they might not necessarily evolve into SE. The low prevalence of atypical absence seizures and atypical absence SE in patients with AS carrying *UBE3A* mutations might be explained by $GABA_AR$ subunit gene expression. In other words, decreased or absent $GABA_AR$ expression in the thalamus might play a critical role in the aggravation of generalized spike-waves and atypical absence seizures in deletion-type AS.

Interestingly, cortical myoclonus observed in our 4 patients was often triggered by specific events, such as changing of clothes, sitting in the toilet, voluntary movements, menstruation, respiratory infections, or emotional changes. Because this aspect of AS has not been studied in detail, future research should examine the precipitating factors of cortical myoclonus in a larger patient population.

Furthermore, the drug piracetam and its analog LEV are effective [4] or ineffective [10] in the treatment of tremors in patients with AS. This was clearly observed in the present report, even in patients with the same 6-bp *UBE3A* deletion. Similar to that observed in patient 2, LEV was effective in controlling nonconvulsive SE in

Please cite this article in press as: Goto M et al. Episodic tremors representing cortical myoclonus are characteristic in Angelman syndrome due to *UBE3A* mutations. Brain Dev (2014), http://dx.doi.org/10.1016/j.braindev.2014.04.005

Table 2
Epilepsies in Angelman syndrome caused by *UBE3A* mutations.

Patient	1	2	3	4
Ictal EEG during tremulous movements	(1) 8–10 Hz augmenting activity with an Fz–Cz predominance at the initial phase(2) Diffuse 2.5–4 Hz slow activity with spike components at the later phase	(1) 8–10 Hz rhythmic activity with an Fz–Cz predominance(2) No apparent EEGchange	6–7 Hz rhythmic activity with Cz predominance	6–8 Hz rhythmic activity with a centroparietal predominance and short spike-wave bursts
Onset of tremulous movements	1 year 1 month	5 years 3 months	2 years 2 months	7 years 2 months
Frequency of tremulous movements	Once an hour	All day	10 times a day	Once in 3 h
Duration of tremulous movements	<10 s	10–50 min	<10 s	⩽3–4 h
Distribution of tremulous movements	Head, upper limbs, trunk	Head, upper and lower limbs	Upper limbs	Upper and lower limbs
Precipitating factors for tremulous movements	Voluntary limb movements, sleepiness, tense, surprise	Changing clothes, irritability	–	Sitting in the toilet, changing clothes or diaper, menstruation
Ineffective medication for tremulous movements	PHT, CLB, CBZ, TPM (dosage not available)	–	VPA (200 mg)LTG (30 mg)	VPA (600 mg), CLZ (30 mg),CLB (20 mg), LEV (3000 mg)
Effective medication for tremulous movements	VPA (300 mg)ESM (400 mg)	VPA (1000 mg), LEV (1000 mg); bromazepam (during irritable period)	LEV (150 mg)	–
Dose escalation of LEV	N/A	7 mg/kg/month	10 mg/kg/month	8 mg/kg/month
Side effects of LEV	N/A	None	None	None
Other seizure types	Isolated myoclonus	–	Atonic (3 times)	Tonic–clonic

CBZ, carbamazepine; CLB, clobazam; CLZ, clorazepate; ESM, ethosuximide; LTG, lamotrigine; LEV, levetiracetam; TPM, topiramate; VPA, valproate.
N/A: not applicable.

patients with AS [18]. Although LEV is not effective in all patients with AS, it might be useful in the treatment of intractable epilepsies. We believe that provocation of SE in AS by CBZ and vigabatrin [13] should be broadly recognized.

In conclusion, patients with AS carrying *UBE3A* mutations exhibited tremors resulting from cortical myoclonus. Furthermore, JLA showed cortical potentials that preceded electromyographic activity, irrespective of ictal electroencephalographic results (i.e., no change in background, 8–10 Hz frontocentral activity, or diffuse spike-wave activity). The low prevalence of atypical absence seizures and atypical absence SE in patients with AS carrying *UBE3A* mutations might be explained by preserved $GABA_AR$ subunit gene expression. Levetiracetam is an antiepileptic drug that holds promise for the treatment of epilepsy in patients with AS.

Acknowledgments

Drs. Yoshiaki Saito and Masayuki Sasaki received financial support from the Japanese Ministry of Health, Labour and Welfare (Research Grant for Nervous and Mental Disorders 24-7).

Appendix A. Supplementary data

Supplementary data associated with this article can be found, in the online version, at http://dx.doi.org/10.1016/j.braindev.2014.04.005.

References

[1] Guerrini R, Carrozzo R, Rinaldi R, Bonanni P. Angelman syndrome: etiology, clinical features, diagnosis, and management of symptoms. Paediatr Drugs 2003;5:647–61.
[2] Lossie AC, Whitney MM, Amidon D, Dong HJ, Chen P, Theriaque D, et al. Distinct phenotypes distinguish the molecular classes of Angelman syndrome. J Med Genet 2001;38:834–45.
[3] Fiumara A, Pittalà A, Cocuzza M, Sorge G. Epilepsy in patients with Angelman syndrome. Ital J Pediatr 2010;36:31.
[4] Guerrini R, De Lorey TM, Bonanni P, Moncla A, Dravet C, Suisse G, et al. Cortical myoclonus in Angelman syndrome. Ann Neurol 1996;40:39–48.
[5] Dan B, Chéron G. Postural rhythmic muscle bursting activity in Angelman syndrome. Brain Dev 2004;26:389–93.
[6] Ogawa K, Ohtsuka Y, Kobayashi K, Asano T, Oka E. The characteristics of epilepsy with Angelman syndrome. Epilepsia 1996;37(Suppl. 3):83–4.

Please cite this article in press as: Goto M et al. Episodic tremors representing cortical myoclonus are characteristic in Angelman syndrome due to *UBE3A* mutations. Brain Dev (2014), http://dx.doi.org/10.1016/j.braindev.2014.04.005

[7] Elia M. Myoclonic status in nonprogressive encephalopathies: an update. Epilepsia 2009;50(Suppl. 5):41–4.
[8] Dan B, Boyd SG. Angelman syndrome reviewed from a neurophysiological perspective. The UBE3A-GABRB3 hypothesis. Neuropediatrics 2003;34:169–76.
[9] Moncla A, Malzac P, Livet MO, Voelckel MA, Mancini J, Delaroziere JC, et al. Angelman syndrome resulting from UBE3A mutations in 14 patients from eight families: clinical manifestations and genetic counselling. J Med Genet 1999;36:554–60.
[10] Pelc K, Boyd SG, Cheron G, Dan B. Epilepsy in Angelman syndrome. Seizure 2008;17:211–7.
[11] Bureau M, Tassinari CA. Epilepsy with myoclonic absences. Brain Dev 2005;27:178–84.
[12] Elia M, Guerrini R, Musumeci SA, Bonanni P, Gambardella A, Aguglia U. Myoclonic absence-like seizures and chromosome abnormality syndromes. Epilepsia 1998;39:660–3.
[13] Valente KD, Koiffmann CP, Fridman C, Varella M, Kok F, Andrade JQ, et al. Epilepsy in patients with Angelman syndrome caused by deletion of the chromosome 15q11-13. Arch Neurol 2006;63:122–8.
[14] Matsumoto A, Kumagai T, Miura K, Miyazaki S, Hayakawa C, Yamanaka T. Epilepsy in Angelman syndrome associated with chromosome 15q deletion. Epilepsia 1992;33:1083–90.
[15] Uemura N, Matsumoto A, Nakamura M, Watanabe K, Negoro T, Kumagai T, et al. Evolution of seizures and electroencephalographical findings in 23 cases of deletion type Angelman syndrome. Brain Dev 2005;27:383–8.
[16] Espay AJ, Andrade DM, Wennberg RA, Lang AE. Atypical absences and recurrent absence status in an adult with Angelman syndrome due to the UBE3A mutation. Epileptic Disord 2005;7:227–30.
[17] Moncla A, Malzac P, Voelckel MA, Auquier P, Girardot L, Mattei MG, et al. Phenotype-genotype correlation in 20 deletion and 20 non-deletion Angelman syndrome patients. Eur J Hum Genet 1999;7:131–9.
[18] Weber P. Levetiracetam in nonconvulsive status epilepticus in a child with Angelman syndrome. J Child Neurol 2010;25:393–6.

Please cite this article in press as: Goto M et al. Episodic tremors representing cortical myoclonus are characteristic in Angelman syndrome due to *UBE3A* mutations. Brain Dev (2014), http://dx.doi.org/10.1016/j.braindev.2014.04.005

Report

Cell Reports

The Microtubule-Depolymerizing Activity of a Mitotic Kinesin Protein KIF2A Drives Primary Cilia Disassembly Coupled with Cell Proliferation

Graphical Abstract

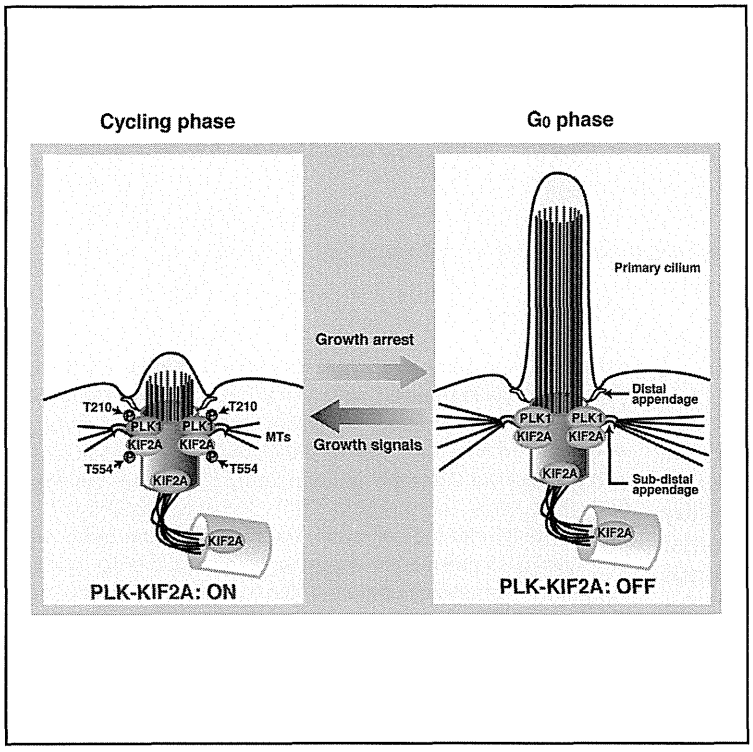

Authors

Tatsuo Miyamoto, Kosuke Hosoba, ..., Brian David Dynlacht, Shinya Matsuura

Correspondence

shinya@hiroshima-u.ac.jp

In Brief

Primary cilium disassembly is coupled with cell proliferation. Miyamoto et al. now find that the PLK1-KIF2A pathway drives physiological cilia disassembly and that its constitutive activation contributes to defective ciliogenesis in PCS syndrome caused by mutation of the *BubR1* gene.

Highlights

- KIF2A is required for primary cilia disassembly
- PLK1 phosphorylates KIF2A to enhance microtubule-depolymerizing activity
- KIF2A is quantitatively controlled by APC/C ubiquitin ligase
- Constitutive activation of PLK1-KIF2A pathway impairs ciliogenesis

Miyamoto et al., 2015, Cell Reports *10*, 1–10
February 10, 2015 ©2015 The Authors
http://dx.doi.org/10.1016/j.celrep.2015.01.003

Please cite this article in press as: Miyamoto et al., The Microtubule-Depolymerizing Activity of a Mitotic Kinesin Protein KIF2A Drives Primary Cilia Disassembly Coupled with Cell Proliferation, Cell Reports (2015), http://dx.doi.org/10.1016/j.celrep.2015.01.003

Cell Reports
Report

The Microtubule-Depolymerizing Activity of a Mitotic Kinesin Protein KIF2A Drives Primary Cilia Disassembly Coupled with Cell Proliferation

Tatsuo Miyamoto,[1] Kosuke Hosoba,[1] Hiroshi Ochiai,[1,2] Ekaterina Royba,[1] Hideki Izumi,[1] Tetsushi Sakuma,[3] Takashi Yamamoto,[3] Brian David Dynlacht,[4] and Shinya Matsuura[1,*]

[1]Department of Genetics and Cell Biology, Research Institute for Radiation Biology and Medicine, Hiroshima University, Hiroshima 734-8553, Japan

[2]Research Center for the Mathematics on Chromatin Dynamics (RcMcD), Hiroshima University, Higashi-Hiroshima 739-8530, Japan

[3]Department of Mathematical and Life Sciences, Graduate School of Science, Hiroshima University, Higashi-Hiroshima 739-8526, Japan

[4]Department of Pathology and Cancer Institute, Smilow Research Center, New York University School of Medicine, 522 1st Avenue, New York, NY 10016, USA

*Correspondence: shinya@hiroshima-u.ac.jp

http://dx.doi.org/10.1016/j.celrep.2015.01.003

SUMMARY

The primary cilium is an antenna-like, microtubule-based organelle on the surface of most vertebrate cells for receiving extracellular information. Although primary cilia form in the quiescent phase, ciliary disassembly occurs when quiescent cells re-enter the proliferative phase. It was shown that a mitotic kinase, Polo-like kinase 1 (PLK1), is required for cell-proliferation-coupled primary cilia disassembly. Here, we report that kinesin superfamily protein 2A (KIF2A), phosphorylated at T554 by PLK1, exhibits microtubule-depolymerizing activity at the mother centriole to disassemble the primary cilium in a growth-signal-dependent manner. *KIF2A*-deficient hTERT-RPE1 cells showed the impairment of primary cilia disassembly following growth stimulation. It was also found that the PLK1-KIF2A pathway is constitutively active in cells from patients with premature chromatid separation (PCS) syndrome and is responsible for defective ciliogenesis in this syndrome. These findings provide insights into the roles of the PLK1-KIF2A pathway in physiological cilia disassembly and cilia-associated disorders.

INTRODUCTION

The primary cilium is a microtubule (MT)-based, nonmotile projection located on the surface of most vertebrate cells that senses extracellular information to transduce signals required for cell proliferation, embryogenesis, and tissue homeostasis (Ishikawa and Marshall, 2011). Dysfunctions of primary cilia cause ciliopathies characterized by a range of clinical symptoms including polycystic kidney, obesity, neuronal, and other developmental abnormalities (Nigg and Raff, 2009). The dynamics of primary cilia assembly and disassembly is tightly controlled throughout the cell cycle (Tucker et al., 1979). In the G0 quiescent phase, the centrosome migrates to the apical cell surface, where the mother centriole is transformed to a basal body, with subsequent assembly of the primary cilium from the basal body (Kobayashi and Dynlacht, 2011; Nigg and Stearns, 2011). Upon re-entry into the cell cycle, the primary cilium disassembles quickly to release the centrioles to form a bipolar spindle assembly, suppressing primary cilium formation during the proliferative phase (Kobayashi and Dynlacht, 2011; Nigg and Stearns, 2011). In contrast to primary cilia assembly, little is known about the molecular basis underlying the induction of primary cilia disassembly and blocking of inappropriate ciliogenesis in the proliferative phase. Recent studies, however, have revealed that a mitotic kinase Polo-like kinase1 (PLK1) plays a pivotal role in growth-signal-dependent primary cilia disassembly (Lee et al., 2012; Seeger-Nukpezah et al., 2012; Wang et al., 2013a). PLK1 phosphorylates histone deacetylase 6 (HDAC6) to promote tubulin deacetylation and to destabilize the axonemal MTs of primary cilia (Wang et al., 2013a). PLK1 also interacts with a Wnt signal component Dishevelled 2 (DVL2) to initiate primary cilia disassembly through the activation of HDAC6 following noncanonical Wnt5a ligand stimulation (Lee et al., 2012). PLK1 regulates many substrates to orchestrate mitotic spindle formation and chromosomal stability (Bruinsma et al., 2012). However, as yet, HDAC6 is the only major PLK1 substrate identified in PLK1-mediated primary cilia disassembly.

The human *kinesin-13* gene family consists of *KIF2A*, *KIF2B*, *KIF2C/MCAK*, and *KIF24* (Walczak et al., 2013). Unlike conventional kinesin motor proteins involved in intracellular transport, kinesin-13 proteins do not "walk" along MTs but have the unique activity of ATP-dependent MT depolymerization (Walczak et al., 2013). The MT-depolymerizing activity of kinesin-13 proteins operates in a range of physiological contexts such as spindle assembly, chromosome segregation, and axonal growth (Ganem and Compton, 2004; Homma et al., 2003; Jang et al., 2009). Recently, it was reported that mammalian KIF24 blocks

Please cite this article in press as: Miyamoto et al., The Microtubule-Depolymerizing Activity of a Mitotic Kinesin Protein KIF2A Drives Primary Cilia Disassembly Coupled with Cell Proliferation, Cell Reports (2015), http://dx.doi.org/10.1016/j.celrep.2015.01.003

ciliogenesis by recruiting CP110 at the mother centrioles and remodeling centriolar MTs through its MT-depolymerizing activity. In addition, small interfering RNA (siRNA)-mediated knockdown of *KIF24* causes inappropriate ciliogenesis even in cycling cells (Kobayashi et al., 2011). However, whether other kinesin-13 proteins are involved in primary cilia formation remains unclear. Previous studies have demonstrated that PLK1-mediated phosphorylation of KIF2A, KIF2B, and KIF2C controls their MT-depolymerizing activity for faithful chromosome segregation and spindle assembly, and the PLK1-phosphorylation sites on KIF2B and KIF2C, but not KIF2A, were identified (Hood et al., 2012; Jang et al., 2009; Zhang et al., 2011). PLK1-related biological links between ciliary disassembly and tuning of kinesin-13-mediated MT depolymerization led us to explore how PLK1 and kinesin-13s cooperate to regulate primary cilia disassembly in the proliferative phase. In this study, we report that PLK1 phosphorylates KIF2A at T554 in the subdistal appendages of the mother centriole to activate its MT-depolymerizing activity and disassemble primary cilia following growth stimulation.

Premature chromatid separation (PCS) syndrome (Mendelian Inheritance in Man [MIM] ID: 176430), also known as mosaic variegated aneuploidy (MVA) syndrome (MIM ID: 257300), is a rare autosomal recessive disorder caused by germline mutations in the *budding uninhibited by benzimidazoles 1 homolog beta* (*BUB1B*) gene, encoding BUBR1, a central player in the mitotic spindle assembly checkpoint (Hanks et al., 2004; Matsuura et al., 2006). The clinical symptoms of PCS (MVA) syndrome patients include a high risk of cancer and symptoms that overlap with the ciliopathy disease spectrum, including polycystic kidney, Dandy-Walker complex, and infantile obesity (Hanks et al., 2004; Matsuura et al., 2006; Miyamoto et al., 2011). We previously demonstrated that skin fibroblasts from these patients show reduced ciliogenesis, thus PCS (MVA) syndrome is defined as a ciliopathy (Miyamoto et al., 2011). Here, we show that the PLK1-KIF2A pathway is dysregulated in cells from PCS (MVA) syndrome patients and that this is a pathological mechanism of the observed ciliopathy disease in this syndrome.

RESULTS

To investigate which kinesin-13 family members have primary cilia disassembly function, we analyzed the effects of exogenous AcGFP1-tagged kinesin-13s on primary cilia formation in serum-starved hTERT-RPE1cells (Figures 1A and 1B). In agreement with a previous report (Kobayashi et al., 2011), exogenous KIF24 formed aggregates in the cytoplasm and suppressed primary cilia to less than 5% (Figures 1A and 1B). We found that exogenous KIF2A, KIF2B, and KIF2C all localized to the centrosomes, and KIF2A and KIF2C, but not KIF2B, reduced ciliated cells to around 10%–20% compared with the control AcGFP1 (Figures 1A and 1B). Given that KIF2A suppressed primary cilia formation more efficiently than KIF2C, we focused on the KIF2A molecule as an effector of PLK1-dependent primary cilia disassembly in this study. KIF2A contains a central catalytic motor domain, an N-terminal neck domain, and a C-terminal stalk domain. The catalytic motor domain contains a MT-depolymerization motif (KVD) and a MT-binding motif (KEC), which are required for MT depolymerization (Figure 1C). The neck domain contains a kinesin-13 family-specific stretch of ~60 highly charged amino acids. The stalk domain is essential for KIF2A dimerization (Figure 1C). We transfected serum-starved hTERT-RPE1 cells with AcGFP1-tagged KIF2A loss-of-function mutants for KEC and KVD (Walczak et al., 2013) and evaluated the effect on ciliogenesis. Mutants for KEC, KVD, and KEC/KVD all localized to the centrosome but failed to reduce ciliated cells (Figure 1D). These results suggested that the MT-depolymerizing activity of KIF2A at the basal body is required for primary cilia suppression.

To precisely determine the localization of KIF2A in the quiescent G0 phase, we stained endogenous KIF2A in hTERT-RPE1 cells with anti-KIF2A antibody. Three KIF2A-positive spots at the mother centriole and one KIF2A-positive spot at the daughter centriole were observed. These colocalized with ninein signals, which correspond to the subdistal appendages of the mother centriole and the proximal ends of both centrioles, but did not exactly colocalize with the centrosomal signals of γ-tubulin (Figure 1E). KIF24 also localized to both centrioles during the G0 phase (Figure S3I). The signals of KIF24 at the mother centriole were partially overlapped with the distal spots of ninein and detected at the more-distal portion residing at subdistal appendages (Figure S3I).

Next, we attempted to identify the PLK1-phosphorylation site on KIF2A associated with primary cilia disassembly. KIF2A contains three conserved motifs for PLK1 phosphorylation (D/E-X-S/T-X_{1-3}-X-D/E; Nakajima et al., 2003). To test whether any of these PLK1 motifs are required for primary cilia suppression, we constructed AcGFP1-tagged alanine-substituted mutants (S37A, T554A, or T558A), which were expected to reduce the MT-depolymerizing activity of KIF2A. We introduced them into serum-starved hTERT-RPE1 cells and counted ciliated cells. Although the S37A and T558A mutants showed similar activity to wild-type KIF2A, the T554A KIF2A mutant did not reduce the numbers of primary cilia observed to the same extent (Figures 2A and 2B). These results suggested that the T554 residue is involved in the KIF2A-mediated primary cilia suppression. The percentage of ciliated cells expressing KIF2A-T554A was also significantly different from the control AcGFP1 (Figure 2B), suggesting a residual (basal) activity of this mutant for primary cilia suppression independently of Plk1 phosphorylation. To confirm that this residue is indeed the PLK1-phosphorylation target, we performed an in vitro kinase assay with His-tagged PLK1 and glutathione S-transferase (GST)-tagged KIF2A, the T558A mutant or the predicted phosphoresistant T554A mutant. Wild-type KIF2A and the T558A mutant were phosphorylated by PLK1. On the other hand, the T554A mutant showed intermediate level of PLK1 phosphorylation between control and the wild-type KIF2A (Figure 2C). These results suggested that T554 on KIF2A is at least one of the PLK1-phosphorylation sites. We then examined whether the MT-depolymerizing activity of KIF2A is regulated by PLK1 phosphorylation of T554 on KIF2A using an in vitro MT-depolymerization assay. Recombinant KIF2A, KIF2A T554A, or KIF2A phosphomimetic mutant (T554E) mutant were purified and mixed with PLK1 and ATP and then with Taxol-polymerized MTs. The reaction mixtures were fractionated using ultracentrifugation, with the remaining MTs found in pellets and depolymerized tubulins in supernatants. Recombinant KIF2A and PLK1 did

Please cite this article in press as: Miyamoto et al., The Microtubule-Depolymerizing Activity of a Mitotic Kinesin Protein KIF2A Drives Primary Cilia Disassembly Coupled with Cell Proliferation, Cell Reports (2015), http://dx.doi.org/10.1016/j.celrep.2015.01.003

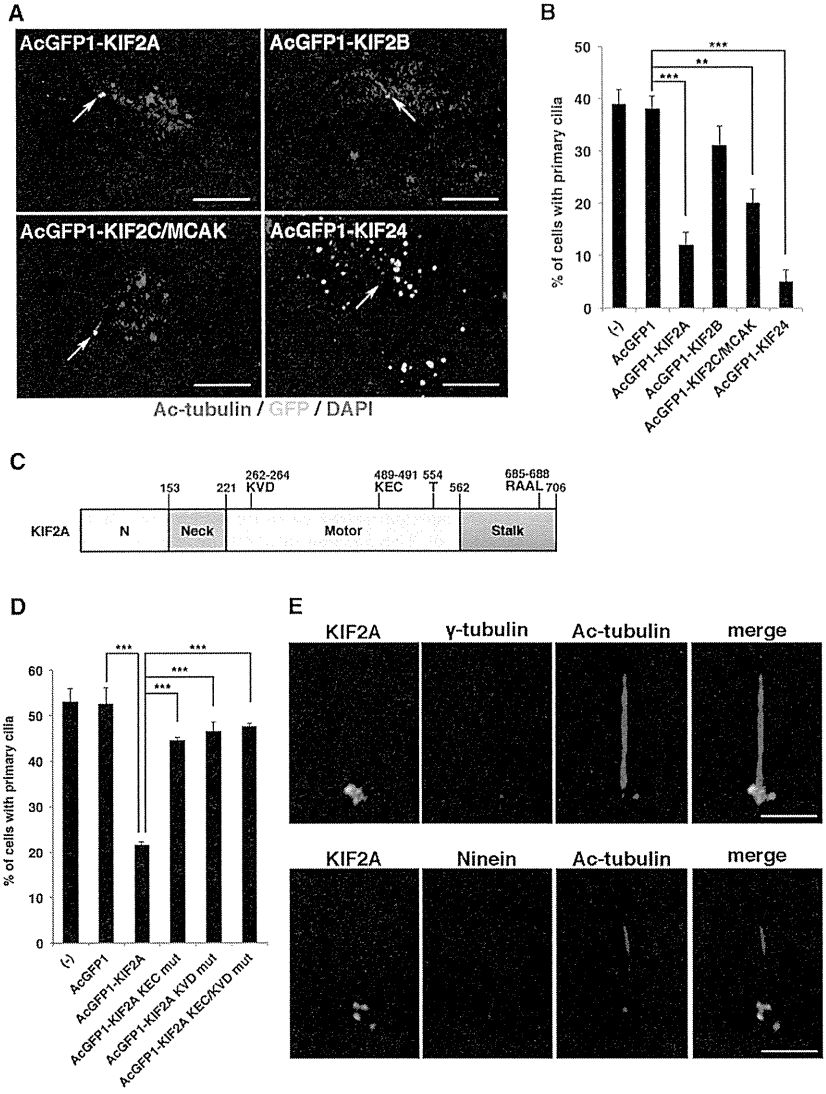

Figure 1. KIF2A Promotes Primary Cilia Disassembly through Microtubule-Depolymerizing Activity

(A) hTERT-RPE1 cells transfected with plasmids expressing AcGFP1-tagged KIF2A, KIF2B, KIF2C/MCAK, or KIF24 and incubated for 24 hr without serum were immunostained with anti-GFP (green) and anti-acetylated tubulin (red) antibodies. DNA was stained with DAPI (blue). Arrow indicates the centrosome/basal body. The scale bar represents 10 μm.

(B) The percentage of hTERT-RPE1 cells with primary cilium from (A) was significantly reduced upon exogenous KIF2A, KIF2C, or KIF24 expression (means ± SD; $^{**}p < 0.01$; $^{***}p < 0.001$; t test; n = 3; >200 cells per experiment).

(C) Schematic of KIF2A structure. The neck domain is a kinesin-13-family-specific stretch of ~60 amino acids. The central catalytic motor domain contains a MT-depolymerization motif (KVD), a MT-binding motif (KEC), and the PLK1-phosphorylation residue (T554). An APC/C recognition motif, D-box (RAAL), is located in the stalk domain (see also Figure S1). The stalk domain is necessary for KIF2A dimerization.

(D) Mutations in either or both the microtubule-binding motif (KEC) and microtubule-depolymerizing motif (KVD) of KIF2A decreased the negative activity of ciliogenesis in quiescent hTERT-RPE1 cells (means ± SD; $^{***}p < 0.001$; t test; n = 3; >200 cells per experiment).

(E) Immunofluorescence staining of hTERT-RPE1 cells in quiescent G0 phase with anti-KIF2A (green), anti-acetylated-tubulin (blue), and anti-ninein (red) or anti-γ-tubulin (red) antibodies. KIF2A colocalized with ninein, but not with γ-tubulin. The scale bar represents 2.5 μm.

not exhibit pelleting in the absence of MTs (data not shown), whereas they were coprecipitated with MTs (Figure 2D). KIF2A alone induced the depolymerization of MT, suggesting KIF2A has a basal and PLK1-independent activity for MT depolymerization. Incubation of KIF2A with PLK1 enhanced the MT-depolymerizing activity of KIF2A, whereas KIF2A T554A did not effectively depolymerize Taxol-polymerized MTs even in the presence of PLK1 (Figures 2D and 2E). KIF2A T554E alone showed the MT-depolymerizing activity similar to that of PLK1-treated wild-type KIF2A (Figures 2D and 2E). We concluded that PLK1 phosphorylates KIF2A at T554 to promote MT depolymerization.

To examine how PLK1-mediated phosphorylation of KIF2A is regulated in the context of primary cilia disassembly, we raised anti-phospho-KIF2A (T554) polyclonal antibody and analyzed the centrosomal localization of phosphorylated KIF2A. We first validated that the antibody specifically recognized KIF2A phosphorylated at T554, but not the KIF2A T554A mutant (Figure 3A), and that the level of phosphorylated KIF2A in the whole-cell lysate of BI2536-treated hTERT-RPE1 cells was decreased (Figure S4A). We next examined the precise localization of KIF2A by immunostaining at 0 hr and 4 hr following serum stimulation of 24 hr serum-starved hTERT-RPE1 cells. Total KIF2A signals were detected at both the mother and daughter centriole at all time points (Figure 3B). In contrast, phospho-KIF2A (T554) signals became increasingly enriched in the subdistal appendages of the mother centriole following serum stimulation and were decreased by treatment with BI3536, a PLK1 inhibitor (Figure 3C). Phospho-PLK1 (T210) signals showed similar temporal and spatial localization to those of phospho-KIF2A (T554; Figure 3D). These data demonstrate that PLK1 at the subdistal appendages phosphorylates KIF2A at T554 in a growth-signal-dependent manner. BI2536 treatment impaired suppression of primary cilia by wild-type KIF2A (Figures 3E and 3F). To evaluate the KIF2A T554 phosphorylation effect on ciliogenesis, we introduced KIF2A phosphomimetic mutant (T554E) into serum-starved hTERT-RPE1 cells. Even in the presence of BI2536, exogenous KIF2A T554E reduced

Please cite this article in press as: Miyamoto et al., The Microtubule-Depolymerizing Activity of a Mitotic Kinesin Protein KIF2A Drives Primary Cilia Disassembly Coupled with Cell Proliferation, Cell Reports (2015), http://dx.doi.org/10.1016/j.celrep.2015.01.003

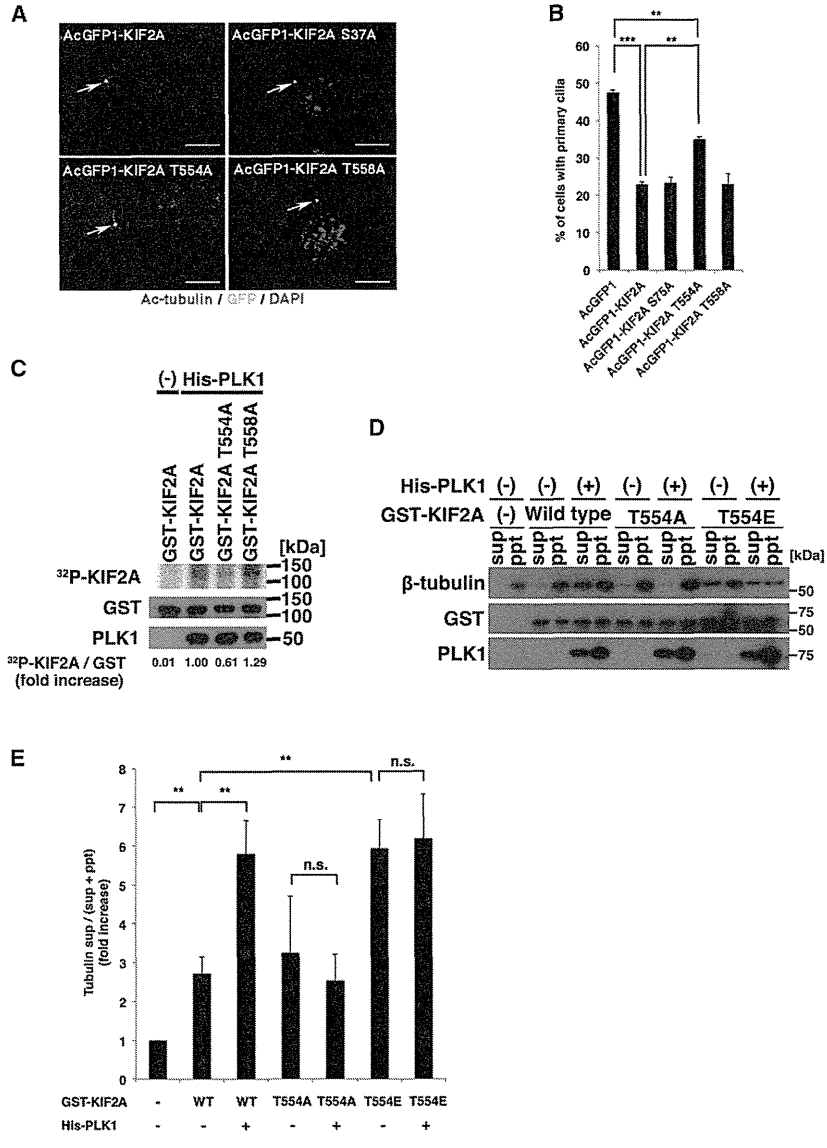

Figure 2. PLK1 Phosphorylates KIF2A at Thr 554 to Enhance Microtubule Depolymerization and Primary Cilia Disassembly

(A) hTERT-RPE1 cells were transfected with AcGFP1-tagged KIF2A or AcGFP1-tagged KIF2A with alanine substitutions at PLK1 phosphorylation consensus sites, serum starved for 24 hr, and then immunostained with anti-GFP (green) and anti-acetylated-tubulin (red) antibodies. DNA was stained with DAPI (blue). Arrow indicates the centrosome/basal body. The scale bar represents 10 μm.

(B) Percentage of cells with primary cilia in GFP-positive cells from (A). The T554A mutation of KIF2A significantly diminished the negative effect on ciliogenesis by KIF2A (means ± SD; $^{**}p < 0.01$; $^{***}p < 0.001$; t test; n = 3; >200 cells per experiment).

(C) In vitro kinase assay to validate the PLK1-mediated phosphorylation site on KIF2A. GST-tagged KIF2A, KIF2A T554A, or KIF2A T558A were incubated with His-tagged PLK1 and γ-^{32}P-ATP and analyzed by autoradiography. Western blotting indicates the loading level of PLK1 and GST-tagged proteins. The level of ^{32}P-uptake into GST-tagged KIF2A recombinants was normalized to GST.

(D) GST-tagged KIF2A, KIF2A T554A, and KIF2A T554E were phosphorylated with His-PLK1 and incubated with Taxol-stabilized microtubules for 10 min. The reaction mix was centrifuged at 100,000 g for 30 min to separate depolymerized tubulin (sup) and microtubule (ppt) fractions, followed by detection of tubulin, KIF2A, and PLK1 with western blotting.

(E) The fold increase of the ratios of tubulin in the supernatant to total input of tubulin [tubulin sup/(sup + ppt)] was calculated. Data from three independent experiments were shown. Error bars represent SD. PLK1 enhanced the MT-depolymerizing activity of wild-type KIF2A, but not KIF2A T554A (means ± SD; $^{**}p < 0.01$; t test). KIF2A T554E effectively depolymerized MTs even in the absence of PLK1. n.s., not significant; WT, wild-type.

ciliated hTERT-RPE1 cells compared with KIF2A and its phosphoresistant mutant (T554A; Figures 3E and 3F), suggesting that the T554E substitution enhances the basal activity of KIF2A for suppressing primary cilia formation. Mutations in the MT-binding motif (KEC) and MT-depolymerizing motif (KVD) abolished the phosphomimetic mutation effect on ciliogenesis (Figures 3E and 3F). Taken together, KIF2A is phosphorylated at T554 by PLK1 in the subdistal appendages of the mother centriole, which enhances MT depolymerization to disassemble primary cilia in a growth-signal-dependent manner.

We investigated the levels of phospho-KIF2A (T554) and total KIF2A in the quiescent or proliferating hTERT-RPE1 cells by western blot analysis. Both the levels of phospho-KIF2A (T554) and total KIF2A normalized by GAPDH were increased in a growth-stimulation-dependent manner (Figure S1A), but the increased rates were different. These results suggested that the half-life of KIF2A is distinctly regulated during the cell cycle. Therefore, we speculated that KIF2A is differently ubiquitinated in quiescent compared with proliferating hTERT-RPE1 cells. As expected, KIF2A was polyubiquitinated in the quiescent G0 phase, whereas the ubiquitination level in the cycling phase was decreased (Figure S1B). Because kinesin-13s contain consensus sequences for the destruction box (D-box: RXXL), which is recognized by anaphase-promoting complex/cyclosome (APC/C) ubiquitin ligase, we explored a physical interaction between kinesin-13s and an APC/C component, CDC27, using immunoprecipitation analysis with anti-FLAG antibody in HEK293T cells transfected with 3× FLAG-tagged kinesin-13s. All members of the kinesin-13 family were able to bind to CDC27 (Figure S1C), suggesting that KIF2A is polyubiquitinated

by APC/C. We constructed three D-box mutants for KIF2A by substituting RXXL in the D-box with AXXA. Mutation of RAAL in the D-box 3 at 685–688 amino acids (aas) inhibited its ubiquitination (Figure S1E), indicating that APC/C recognizes the D-box 3 of KIF2A. The D-box mutation did not alter the centrosomal localization but enhanced the ciliary disassembly activity of KIF2A, whereas this effect was abrogated by mutations within the MT-binding and depolymerizing motifs (Figures S1F and S1G). We thus concluded that KIF2A is degraded through the APC/C-mediated ubiquitin/proteasome system in the quiescent G0 phase.

To explore the physiological function of human KIF2A more precisely, we examined the effect of disruption of *KIF2A* on primary cilia disassembly following growth stimulation and suppression of ciliogenesis during the proliferative phase. We constructed expression vectors encoding transcription-activator-like effector nucleases (TALENs) to introduce DNA double-strand breaks into human *KIF2A* exon 10, corresponding to 291–321 aas in the functional P loop (Figures S2A and S3A). Targeting vectors were designed to disrupt the *KIF2A* gene by replacing exon 10 with a gene cassette of a herpes simplex virus thymidine kinase gene and neomycin- or puromycin-resistant genes separated by a 2A peptide sequence, allowing expression of the distinct proteins from a single open reading frame. After transfection and selections by puromycin and neomycin in hTERT-RPE1 cells, one heterozygous (*KIF2A* +/−) and four homozygous (*KIF2A* −/−) mutant cell clones were obtained. Southern blot analysis confirmed the disruption of the *KIF2A* gene without random integration of the targeting vectors (Figures S2B and S3B). RT-PCR, western blotting, and immunostaining analyses using anti-KIFA2A and anti-phospho-KIF2A (T554) antibodies all showed no KIF2A products in the two *KIF2A* −/− cells (Figures S2C–S2E, S3C, S4A, S4C, and S4D). Therefore, the two *KIF2A* −/− clones were used for subsequent studies.

The frequency and length of primary cilia were examined in 24 hr serum-starved *KIF2A* −/− cells. They showed no significant change in ciliogenesis compared with those of *KIF2A* +/+ cells (Figures S2F, S2G, S3D, and S3E). After serum stimulation, primary cilia disassembly was delayed in *KIF2A* −/− cells (Figures S2F, S2G, S3D, and S3E), indicating that KIF2A is required for primary cilia disassembly following growth stimulation. *KIF2A* −/− cells also showed impaired blocking of inappropriate primary cilia formation during the cycling phase (Figures S3F and S3G). However, *KIF2A*-deficient cells were not able to completely attenuate primary cilia disassembly and blocking of inappropriate ciliogenesis (Figures S2F, S2G, S3F, and S3G). An immunoprecipitation experiment indicated that KIF2A potentially interacts with CP110, which is a binding molecule of KIF24 for blocking aberrant ciliogenesis (Figure S1D). The centriolar localizations of KIF24 and CP110 were not altered in *KIF2A* −/− cells (Figures S3H and S3I), suggesting that KIF24 in *KIF2A* −/− cells redundantly plays a role of blocking ciliogenesis during the cycling phase. Most of *KIF2A* −/− hTERT-RPE1 cells showed normal bipolar spindle formation, whereas a small fraction of them had multipolar spindle (Figures S4E and S4F). Depletion of *KIF2A* in hTERT-RPE1 cells did not significantly affect cell-cycle progression, as determined by flow cytometry (Figure S4G). These data suggest that ciliary phenotypes in *KIF2A* −/− cells are not secondary to the abnormalities of mitosis and cell-cycle progression.

In PCS (MVA) patient cells, PLK1 was aberrantly activated throughout the cell cycle (Figure 4A; Izumi et al., 2009). We therefore examined whether reduced ciliogenesis in the patient cells is owing to the constitutive activation of PLK1. PLK1 inhibition with siRNA or BI2536 partially restored primary cilia formation in the patient cells (data not shown), suggesting that aberrant PLK1 activity contributes to defective ciliogenesis in PCS (MVA) syndrome. To address whether the deregulation of KIF2A in the patient cells contributes to the pathological mechanism, the expression and phosphorylation levels of KIF2A were examined by western blotting analysis. In patient (PCS1) cells transferred with a whole chromosome 15 containing the *BUB1B* locus (PCS1-Ch.15 cells), the expression level of KIF2A gradually increased from G1 to M phase, with T554 phosphorylation strongly detected in M phase, correlating with PLK1 dynamics in the cell cycle (Figure 4A). In contrast, in PCS1 cells, KIF2A was highly expressed and phosphorylated at T554 throughout the cell cycle (Figure 4A), suggesting that KIF2A is involved in the defective ciliogenesis observed in patient cells. Consistent with this, siRNA-mediated knockdown of *KIF2A* in PCS1 cells resulted in partial recovery of primary cilia formation (Figures 4B–4D). A double knockdown of *PLK1* and *KIF2A* increased cilia restoration compared with *PLK1* or *KIF2A* siRNA-mediated knockdown alone (Figures 4B–4D), suggesting that a constitutively active PLK1-KIF2A molecular pathway is underlying the ciliopathy spectrum in PCS (MVA) syndrome. Based on these results, we propose a model where (1) in the quiescent G0 phase, the enzymatic activity of PLK1 and KIF2A is negatively regulated to allow primary cilia assembly and (2) growth signals are transmitted to the PLK1-KIF2A cascade to enhance the MT-depolymerizing activity of KIF2A at the mother centriole for cell-proliferation-coupled primary cilia disassembly (Figure 4E).

DISCUSSION

Primary cilia disassembly following growth stimulation is a critical step in cell proliferation because the basal body/centrosome beneath the cell membrane must be released to act as a mitotic bipolar spindle pole. However, the mechanism by which primary cilia disassembly is coupled with cell proliferation is less well understood. Here, we found that KIF2A promotes primary cilia disassembly via its MT-depolymerizing activity in a growth-signal-dependent manner. It has been established that metazoan KIF2A localizes to mitotic spindle MTs and poles (Figure S3C) and controls spindle assembly and poleward MT flux for proper chromosome segregation through its MT-depolymerizing activity (Ganem and Compton, 2004; Jang et al., 2009). Studies in *KIF2A*-knockout mice showed that KIF2A in postmitotic neurons regulates the number and length of collateral branches from an axon (Homma et al., 2003; Maor-Nof et al., 2013), indicating the existence of nonmitotic functions of KIF2A. Interestingly, ancient kinesin-13 members in *Giardia*, *Leishmania*, and *Chlamidomonas* regulate flagellar length (Blaineau et al., 2007; Dawson et al., 2007; Piao et al., 2009; Wang et al., 2013b). Importantly, it was reported that human KIF24 suppresses inappropriate ciliogenesis in proliferating cells by

OPEN ACCESS
CellPress

Please cite this article in press as: Miyamoto et al., The Microtubule-Depolymerizing Activity of a Mitotic Kinesin Protein KIF2A Drives Primary Cilia Disassembly Coupled with Cell Proliferation, Cell Reports (2015), http://dx.doi.org/10.1016/j.celrep.2015.01.003

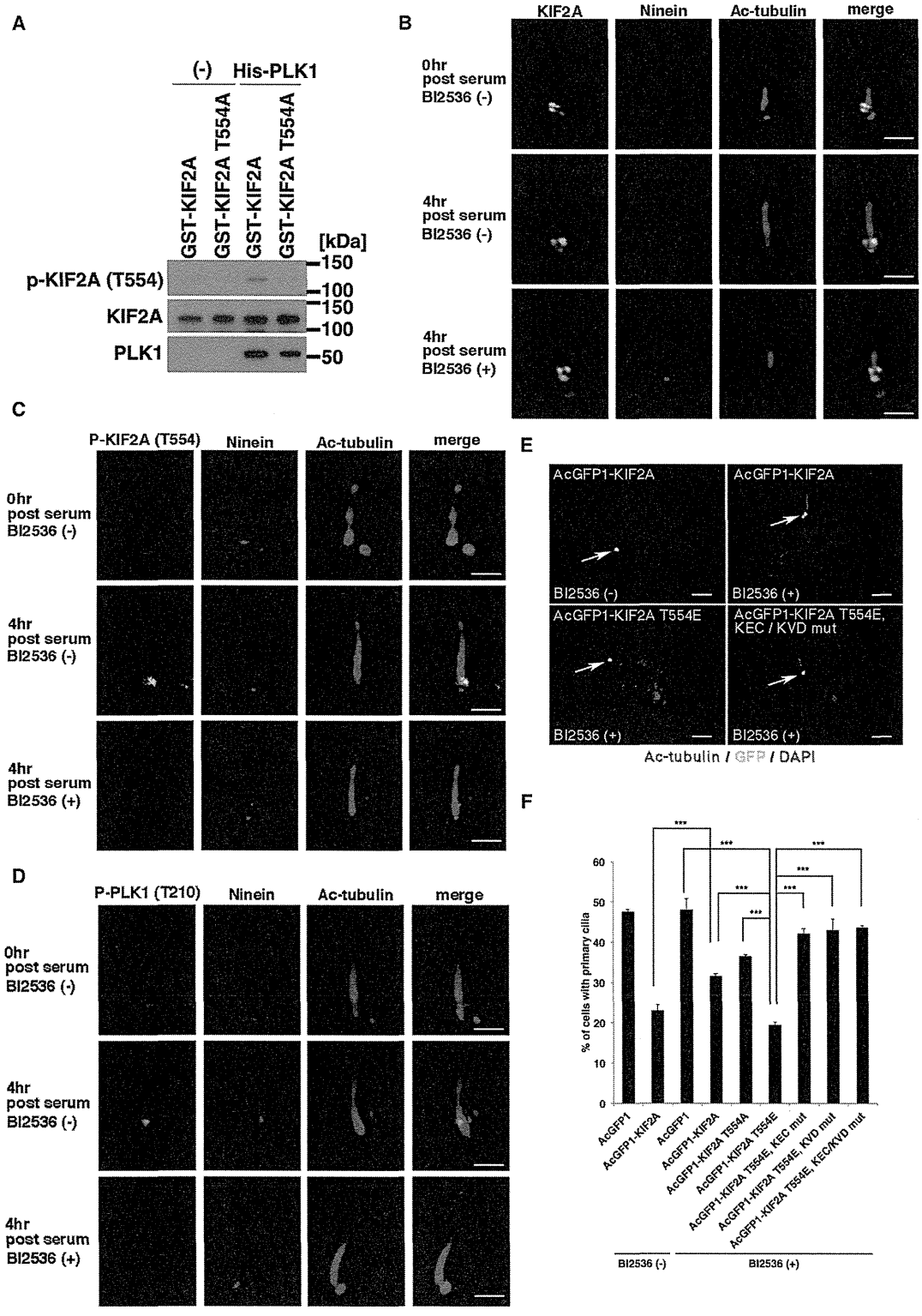

(legend on next page)